analytical chemistry

pubs.acs.org/ac Article

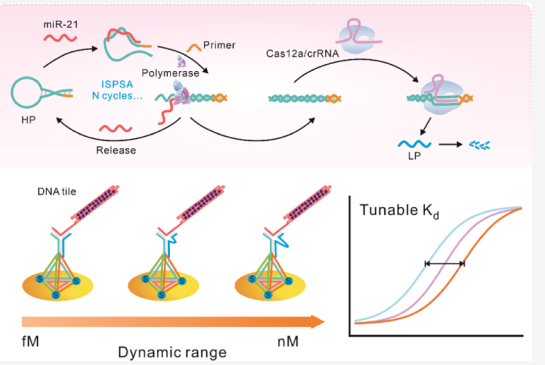
DNA Tile and Invading Stacking Primer-Assisted CRISPR–Cas12a Multiple Amplification System for Entropy-Driven Electrochemical Detection of MicroRNA with Tunable Sensitivity

Huan Wang, Yan Lei Li, Ya Jie Fan, Jiang Xue Dong, Xiang Ren, Hongmin Ma, Dan Wu, Zhong Feng Gao,* Qin Wei, and Fan Xia

Cite This: https://doi.org/10.1021/acs.analchem.3c02603 Read Online

ACCESS | Metrics & More | Article Recommendations | Supporting Information

ABSTRACT: Conventional electrochemical detection of microRNA (miRNA) encounters issues of poor sensitivity and fixed dynamic range. Here, we report a DNA tile and invading stacking primer-assisted CRISPR–Cas12a multiple amplification strategy to construct an entropy-controlled electrochemical biosensor for the detection of miRNA with tunable sensitivity and dynamic range. To amplify the signal, a cascade amplification of the CRISPR–Cas12a system along with invading stacking primer signal amplification (ISPSA) was designed to detect trace amounts of miRNA-31 (miR-31). The target miR-31 could activate ISPSA and produce numerous DNAs, triggering the cleavage of the single-stranded linker probe (LP) that connects a methylene blue-labeled DNA tile with a DNA tetrahedron to form a Y-shaped DNA scaffold on the electrode. Based on the decrease of current, miR-31 can be accurately and efficiently detected. Impressively, by changing the loop length of the LP, it is possible to finely tune the entropic contribution while keeping the enthalpic contribution constant. This strategy has shown a tunable limit of detection for miRNA from 0.31 fM to 0.56 pM, as well as a dynamic range from ~2200-fold to ~270,000-fold. Moreover, it demonstrated satisfactory results in identifying cancer cells with a high expression of miR-31. Our strategy broadens the application of conventional electrochemical biosensing and provides a tunable strategy for detecting miRNAs at varying concentrations.



INTRODUCTION

MicroRNA (miRNA), a kind of noncoding RNA, is naturally produced and consists of short, single-stranded sequences, which has the ability to specifically bind to matching mRNA and prevent gene transcription.[1−3] Many investigations have revealed that the levels of miRNA expression relate strongly to a range of human illnesses, such as infectious diseases, neurodegenerative disorders, diabetes, and a variety of cancers.[4−6,7] Thus, the sensitive determination of cancer-related miRNAs is highly essential for the diagnosis and timely therapy of cancer in early stages.[1] The most commonly used protocol for RNA detection is quantitative reverse transcription-polymerase chain reaction (qRT-PCR),[8] and microarrays and Northern blotting are also utilized.[9] These techniques, however, have limitations including large sample volumes, time-consuming operations, complicated primer constructions, and sophisticated equipment, which hinder their use in practical applications. Recently, various biosensing strategies have been developed, such as the use of a CRISPR–Cas12a system, which is a class II CRISPR–Cas system that includes CRISPR RNA (crRNA) and Cas12a nuclease and has been effectively used as a diagnostic tool for detecting miRNAs.[10−12] The CRISPR–Cas12a sensing systems have been designed to improve sensitivity using DNA barcodes, DNA tetrahedrons, DNA walkers, hybrid chain reactions, liposomes, and functional nanomaterials.[13−17] For example, Song and colleagues developed a DNA-barcoded metal–organic framework combined with CRISPR–Cas12a for miRNA detection, which holds great promise in clinical diagnosis.[13] Li and colleagues proposed a liposome-based CRISPR–Cas12a strategy for the surface-enhanced Raman scattering and naked-eye detection of DNA fragments with high sensitivity down to the attomolar level.[14] Integrating functional materials, such as nanozymes,[18] MXene,[19] gold nanoparticles, and so on, with CRISPR–Cas12a has promoted the investigation of sensitive detection strategies. Although these methods showed significant biosensing performance, they still suffer from some major disadvantages including high

Received: June 14, 2023
Accepted: August 11, 2023

Downloaded via SHANGHAI NORMAL UNIV on August 27, 2023 at 05:18:47 (UTC).
See https://pubs.acs.org/sharingguidelines for options on how to legitimately share published articles.

© XXXX American Chemical Society

nonspecific backgrounds, complicated probe designs, and time-consuming processes. Interestingly, DNA tile self-assembly nanostructure has exceptional potential in bioassays because of its programmability, structural rigidity, simple preparation, physiological stability, and robust signal loading capacity.[20,21] However, most studies on DNA tiles have primarily focused on the design of the structure, regulation of assembly, targeted diagnosis, and treatments.[22−25] Therefore, developing reliable, sensitive, and specific techniques that integrate the CRISPR−Cas12a reaction with the DNA tile for miRNA detection is still a challenge.

The precise identification of miRNA is crucial for the prevention, treatment, and prediction of cancer. Although numerous detection methods have been developed, most rely on biological recognition mechanisms and have a fixed sensitivity and dynamic range that limit their effectiveness.[26−28] It should be noted that the concentration of nucleic acid varies between different samples, making it difficult to detect different nucleic acids within a fixed dynamic range.[29−31] Thus, it is imperative to develop a highly adjustable and sensitive dynamic range for miRNA analysis. Various natural approaches have recently been utilized to finely adjust the dynamic range of biosensors.[32−35] For example, Porchetta and co-workers demonstrated two methods, namely, distal-site mutation and allosteric inhibition, that change the switching equilibrium constant to adjust the detection performance of aptasensors over several orders of magnitude.[36] Meanwhile, Yang and colleagues proposed controlled DNA valency and enhanced hydrogelation to modify the detection range and yield the limit of detection (LOD) ranging from fM to nM.[29,37] We also developed an enthalpy and entropy synergistic regulated strategy to control the response performance of the DNA motif.[38] The study revealed that by controlling the loop length and mismatched bases in the stem, the acid dissociation constant could be tuned arbitrarily to increase or decrease sensitivity while simultaneously improving the dynamic range. However, the utilization of this thermodynamic approach in the detection of miRNA using signal amplification has not yet been explored.

In this work, a sensitive entropy-driven electrochemical biosensor was developed through the DNA tile and invading stacking-prime-assisted CRISPR−Cas12a signal amplification to detect miRNA-31 (miR-31) as the model target. The invading stacking primer signal amplification (ISPSA) was designed to produce a large number of DNA products when triggered by miR-31. These products then triggered the DNase activity of CRISPR−Cas12a, causing nonspecific single-stranded DNA cleavage and resulting in a low current intensity. Conversely, the inactivated CRISPR−Cas12a allowed single-stranded DNA to hybridize with tetrahedron DNA and DNA tiles to form a Y-shaped DNA scaffold, leading to a high current signal. By regulating the thermodynamic stability of the Y-shaped structure, an entropic contribution was used to fine-tune the detection performance for miR-31. Impressively, the sensitivity was precisely adjusted from 0.31 fM to 0.56 pM with a tunable dynamic range from ∼2200-fold to 270,000-fold. Therefore, this work provides a highly efficient and tunable biosensing system, indicating great potential in detecting biomarkers for early disease diagnosis at trace levels.

EXPERIMENTAL SECTION

Preparation of DNA Tetrahedron-Modified Gold Electrode Surfaces. Gold electrodes were sufficiently cleaned using the procedure in the Supporting Information. A solution of 50 μM was prepared by dissolving four nucleic acid probes, tetrahedrons T, A, B, and C, in tris-HCl buffer solution (10 mM tris-HCl, 0.1 M NaCl, 50 mM $MgCl_2$, pH 8.0). The oligonucleotide sequences are listed in Table S1. By combining 82 μL of tris-HCl buffer and 2 μL of each strand with 10 μL of tris(2-carbozyethyl)phosphine hydrochloride (TCEP, 30 mM), the mixture was heated to 90 °C for 5 min before cooling it to room temperature. The resulting concentration of tetrahedron DNA probes was 1 μM. A cleaned gold electrode was then exposed to 5 μL of DNA tetrahedron overnight at 25 °C. The obtained electrode was carefully washed with phosphate-buffered saline (PBS, 0.01 M), and the surface density was evaluated using the reported approach,[39] resulting in a density of 3.5×10^{12} tetrahedra·cm^{-2}.

Preparation of DNA Tiles. The DNA tiles were assembled following a previous report with some modifications. Initially, DNA probes a−e (2 μM) were added in tris acetate-EDTA buffer solution (40 mM tris acetate, 12.5 mM $MgCl_2$, 1 mM EDTA, pH 8.0). Subsequently, the mixture was heated to 90 °C and allowed to cool down for 6 h until it reached 25 °C to obtain DNA tiles for further use.

Reaction Procedure for Detecting miRNA. First, the ISPSA technique was employed, using a 20 μL system solution containing different concentrations of miR-31 (10 μL), 1 μL of dNTPs (10 mM), and different concentrations of polymerase, primers, and HP probes. The mixture was kept at a physiological temperature for 20 min of incubation. Subsequently, the CRISPR−Cas12a reaction process was carried out after ISPSA. The designed crRNA was combined with double-stranded DNA (dsDNA, created by ISPSA), along with a 1× NEB reaction buffer and the LP probe (1 μM) in the reaction solution. This was then treated for 40 min at 37 °C before the enzyme was inactivated by incubating the product at 80 °C for 20 min. The resultant (5 μL) was mixed with DNA tile (5 μL) and then treated with a DNA tetrahedron-modified electrode for 30 min. Afterward, the electrode was carefully washed with phosphate-buffered solution (1×) before the alternating current voltammetry (ACV) measurement.

Thermodynamic Analysis of Thermal Melting Curves. There was general acquiescence that the Y-shaped DNA had constant ΔH° and $\Delta C_p = 0$, allowing it to be temperature-independent, so a two-state model was employed for thermodynamic analysis.[40,41] To obtain α (fraction folded) versus temperature plots, the absorbance data were normalized using the following equation

$$\alpha = (B_{\text{unfold}} - A_T)/(B_{\text{unfolded}} - B_{\text{folded}}) \quad (1)$$

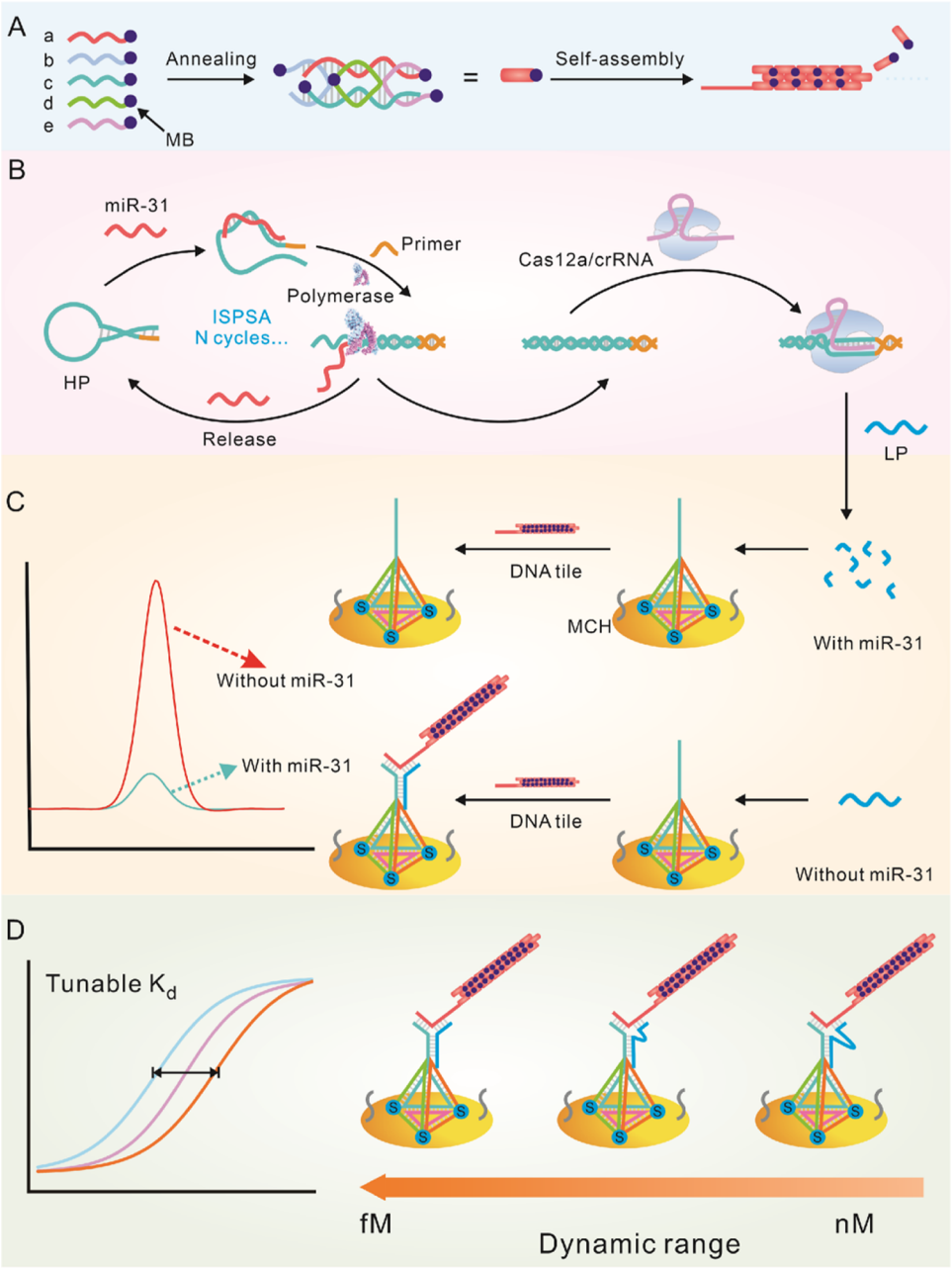
The ultraviolet−visible (UV−vis) absorbance at a specific temperature is denoted as A_T, while the absorbance values of unfolded and folded DNAs are represented by B_{unfolded} and B_{folded}, respectively. The K_{eq} of the melting process can be calculated using the following equation

$$K_{\text{eq}} = \alpha/(1 - \alpha) \quad (2)$$

The α range of 0.10−0.90 was chosen for the analysis because it provided more accurate equilibrium constants within this interval.[42] By graphing the natural logarithm of the equilibrium constant K_{eq} against the inverse temperature ($1/T$ in K), van't Hoff representations were produced. To assess the enthalpic and entropic contributions of Y-shaped DNA, the data from thermal melting curves were fitted with the following equation

https://doi.org/10.1021/acs.analchem.3c02603
Anal. Chem. XXXX, XXX, XXX−XXX

Scheme 1. Schematic Illustration of the Electrochemical Method Using DNA Tile and Invading Stacking Primer-Assisted CRISPR−Cas12a for MiR-31 Detection: (A) Schematic Diagram of the DNA Tile Assembly; (B) Principle for the Cascade Reaction of ISPSA and CRISPR−Cas12a; (C) Schematic Diagram of the Electrochemical Signal Amplification Using DNA Tile; and (D) Schematic Diagram of the Tunable Dynamic Range and Sensitivity by Manipulating the Loop of the Y-Shaped DNA Scaffold



$$\ln(K_{eq}) = -\Delta H/R \times (1/T) + \Delta S/R \quad (3)$$

RESULTS AND DISCUSSION

Mechanism of the Electrochemical Biosensor. Scheme 1 illustrates the schematic diagram of the electrochemical biosensor using a DNA tile and invading stacking primer-assisted CRISPR−Cas12a for the detection of miR-31. First, five methylene blue (MB)-labeled single-stranded DNAs (a−e) are annealed and self-assembled into double-crossover DNA tiles (Scheme 1A). Then, a specific hairpin-DNA (HP) is designed to complement miR-31 (Scheme 1B). When the target is present, the HP opens through nucleic acid hybridization, allowing the invading stacking primer (IS-primer) to combine with the stem of HP. The polymerase assists in extending the IS-primer and replacing the miRNA target, freeing it to hybridize with the opened HP. The ISPSA cyclic reaction converts one target into massive dsDNA, effectively avoiding the need for a thermal cycler. The generated dsDNA activates the DNase activity of CRISPR−Cas12a, leading to the continuous cleavage of the added single-stranded linker probe (LP). To prepare an electrochemical biosensor, a DNA tetrahedron-modified electrode is fabricated (Scheme 1C). The DNA tetrahedron contains an ssDNA

https://doi.org/10.1021/acs.analchem.3c02603
Anal. Chem. XXXX, XXX, XXX−XXX

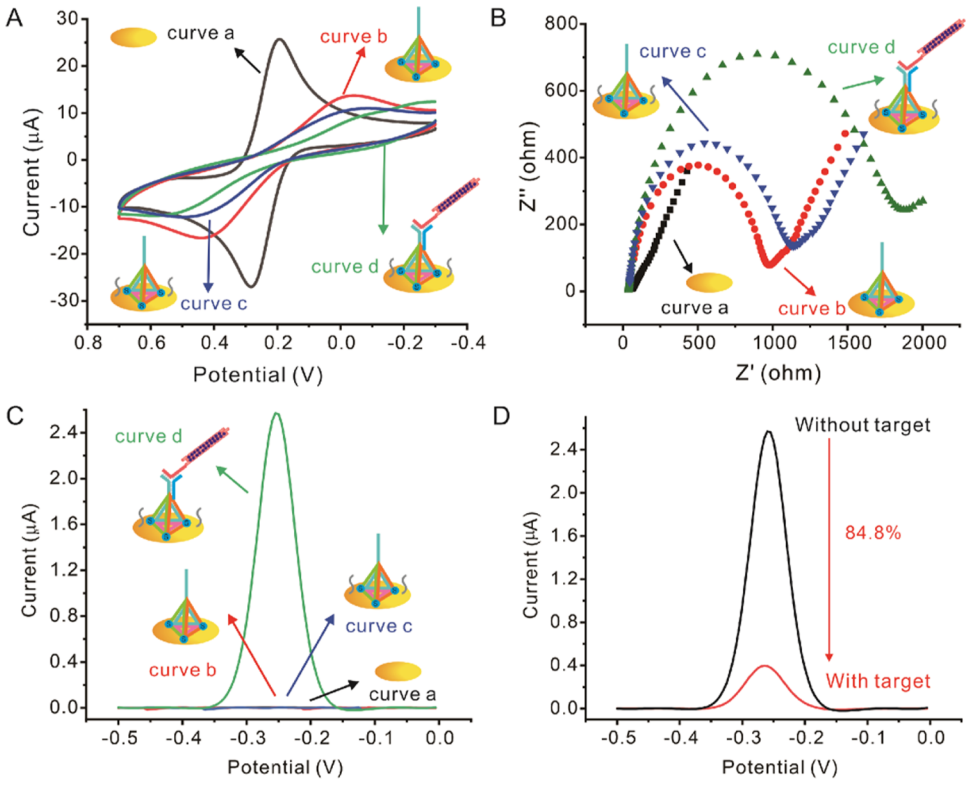


Figure 1. (A) CV, (B) EIS, and (C) ACV curves of the bare gold electrode (a), DNA tetrahedron-modified electrode (b), DNA tetrahedron and MCH-modified electrode (c), and DNA tile-assembled electrode (d). (D) ACV responses of the biosensor in the presence and absence of miR-31.

domain that captures DNA tiles with the aid of LP to form a Y-shaped DNA scaffold. In the absence of miR-31, the reaction activity is efficiently suppressed and LP is well-retained to trap DNA tiles on the electrode surface, leading to a significant current signal. Conversely, the addition of miRNA activates the DNA tile and invades the stacking primer-assisted CRISPR−Cas12a, which then digests LP. This prevents the formation of the Y-shaped DNA scaffold, resulting in a great reduction in the electrochemical intensity. Attributing to the change of current intensity (ΔI), the proposed method can thus enable the sensitive and accurate electrochemical detection of miR-31. Altering the loop length of the Y-shaped DNA scaffold, the detection performances can be well-controlled with tunable dynamic range and sensitivity (Scheme 1D).

Feasibility and Characterization of DNA Tile and Invading Stacking Primer-Assisted CRISPR−Cas12a Amplification Strategy. To investigate the self-assembly of the DNA tile, Figure S1 displays the results of native polyacrylamide gel electrophoresis (PAGE). Lanes 1−5 exhibit distinct single bands of a−e with various migrations. Upon the self-assembly of the five single strands of DNA (a−e) into the DNA tile, a bright band with the highest molecular weight was observed in lane 6, indicating the successful formation of the DNA tile. As shown in Figure S2, the morphology of the DNA tile was further investigated by using atomic force microscopy (AFM). The results revealed the presence of a long DNA tile, exhibiting the typical features of regular tubes, on mica sheets, providing undeniable evidence of the successful assembly of the DNA tile.

DNA tetrahedron is used for fabricating the sensor, which allows for the upright orientation of the recognition probe, thereby ensuring high accuracy and reproducibility in our detection.[43,44] To investigate the stepwise formation of the modified electrochemical biosensor, we utilized cyclic voltammetry (CV) and electrochemical impedance spectroscopy (EIS). As displayed in Figure 1A, the peak current of the DNA tetrahedron (curve *b*) and MCH (curve *c*) experienced a substantial reduction as compared to the bare gold electrode (curve *a*), which was due to the negative charge borne by the phosphate bones of DNA, leading to an unfavorable electrostatic interaction with $[Fe(CN)_6]^{3-/4-}$. Further modification with DNA tiles led to a successive decline of the peak current since DNA tiles restricted the electron transfer (curve *d*). Figure 1B provides additional evidence confirming the successful modification of the electrochemical biosensor through the characterization of the stepwise modification processes using EIS. The bare gold electrode exhibited a slight charge-transfer resistance (R_{ct}) (curve *a*) due to the excellent electrical conductivity of gold, while the R_{ct} values increased sequentially after the stepwise assembly of the DNA tetrahedron (curve *b*), MCH (curve *c*), and DNA tile (curve *d*), which were attributed to the negatively charged DNA. In contrast to the bare (Figure 1C, curve *a*), DNA tetrahedron (curve *b*), and MCH (curve *c*)-modified sensors, the electrochemical biosensor modified with the DNA tile recorded a high current intensity (curve *d*) in the ACV measurements. These results were consistent with those obtained from the CV results, demonstrating the successful preparation of the electrochemical biosensor. In order to investigate the feasibility of the DNA tile and invading stacking-prime-assisted CRISPR−Cas12a for the detection of miR-31, control experiments were conducted. It can be seen from Figure 1D that the blank sample displayed a high current intensity of 2.57 μA, while a low current of 0.39 μA was observed in the presence of 1.0 nM miR-31, indicating a significant signal decrease (84.8%). Moreover, in cases where

https://doi.org/10.1021/acs.analchem.3c02603
Anal. Chem. XXXX, XXX, XXX−XXX

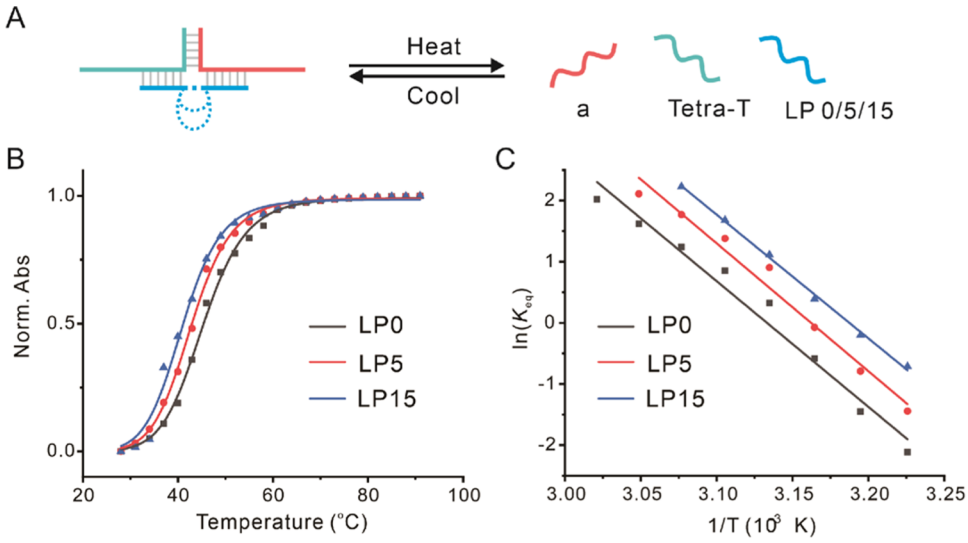


Figure 2. (A) Conformational transformation of the Y-shaped DNA scaffold, (B) melting curves of LP variants, and (C) van't Hoff plot analysis.

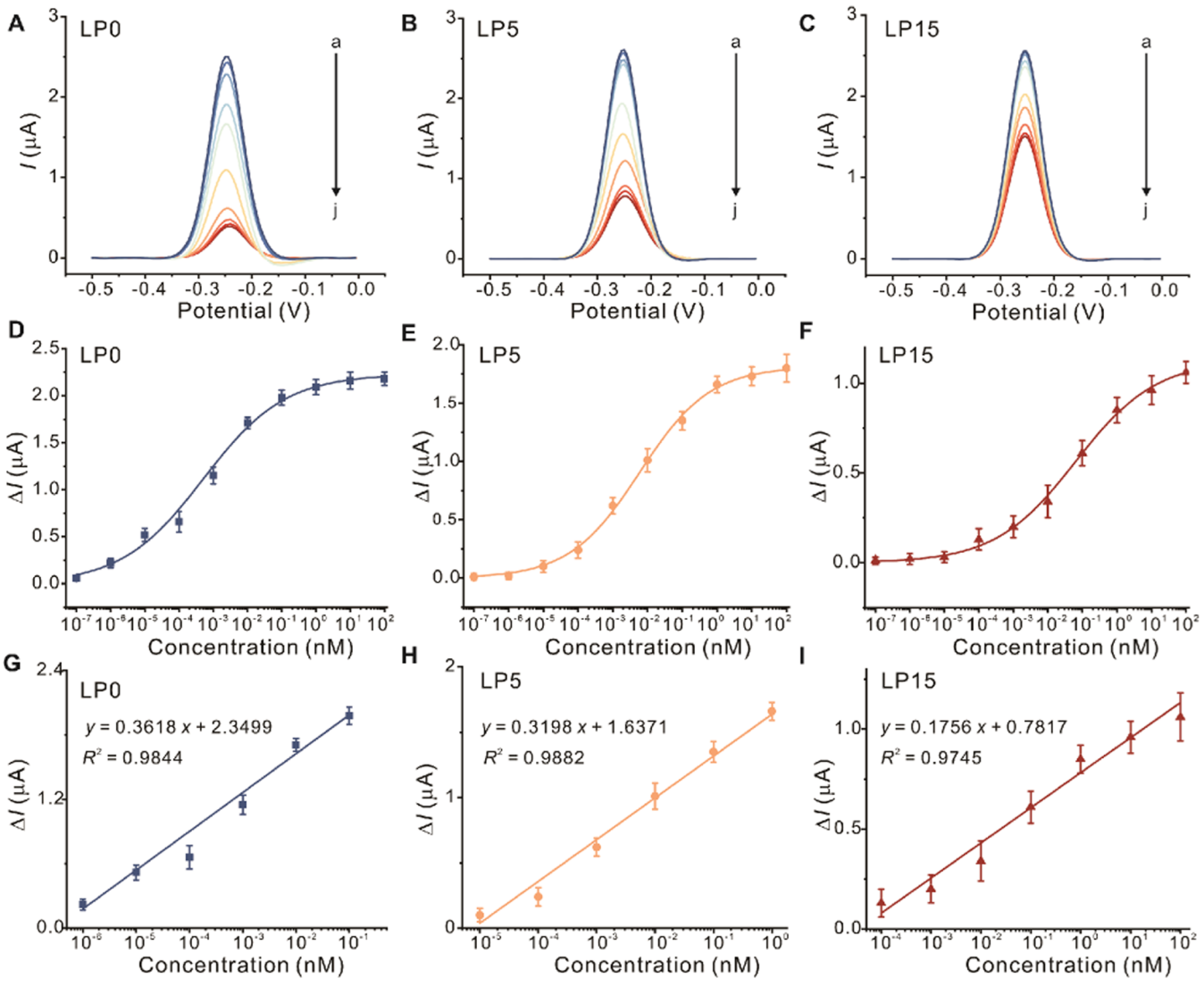


Figure 3. ACV response of the proposed biosensor toward different concentrations of miR-31 using (A) LP0, (B) LP5, and (C) LP15. From panels (a–j): 10^{-7}, 10^{-6}, 10^{-5}, 10^{-4}, 10^{-3}, 10^{-2}, 10^{-1}, 10^{0}, 10^{1}, and 10^{2} nM. The relationship and corresponding linear plots between the change of current intensity and different concentrations of miR-31 using (D, G) LP0, (E, H) LP5, and (F, I) LP15. Error bars indicate the standard deviation of the three replicates.

https://doi.org/10.1021/acs.analchem.3c02603
Anal. Chem. XXXX, XXX, XXX−XXX

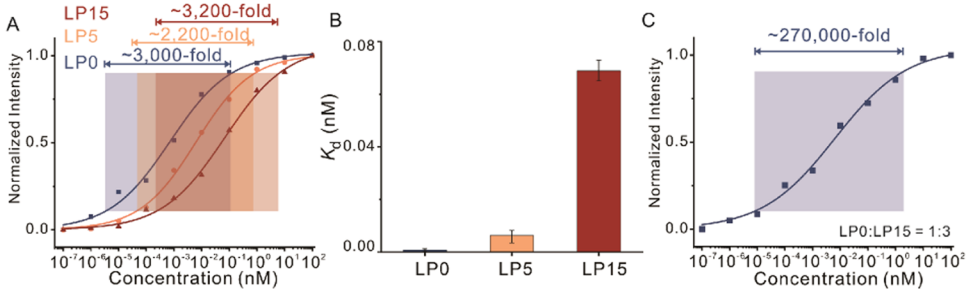


Figure 4. (A) Normalized ACV intensity of the proposed biosensor using different LP variants toward different concentrations of miR-31. (B) The obtained K_d values varied with different LP variants. Error bars indicate the standard deviation of three replicates. (C) The extended dynamic range using the mixture of LP0 and LP15 at a ratio of 1:3.

DNA tiles were not present and only the MB-labeled strand that bound to the target existed, there was only a 42.6% decrease in the current signal (Figure S3). Therefore, the result implied that the DNA tile and invading stacking primer-assisted CRISPR−Cas12a amplification hold great potential to realize the ultrasensitive miRNA detection.

Optimization of the DNA Tile and Invading Stacking Primer-Assisted CRISPR−Cas12a Amplification Strategy. To achieve the optimal biosensing performance of this method, the influence of the concentration of Cas12a protein was first investigated. Figure S4 shows that the current intensity decreased rapidly within the concentration range as the Cas12a protein concentration increased from 1.0 to 5.0 pmol, after which it remained stable. Therefore, an optimal concentration of 5.0 pmol was chosen for subsequent experiments. Figure S5 suggests that the CRISPR−Cas12a system is suitable for reaction after 20 min of ISPSA. If ISPSA is not adequately reacted, the CRISPR−Cas12a system may cleave the miRNA, leading to weak current intensity changes. The strongest changes in intensity occurred at a CRISPR−Cas12a amplification reaction time of 40 min (Figure S6). The optimal time for the DNA tile assembly is demonstrated in Figure S7. The change of the current increased significantly from 10 to 30 min of incubation time and then reached a plateau. This result indicates that 30 min is the best DNA tile assembly time on the electrode for this study. As shown in Figure S8, the short stem length (6 and 9 nt) allowed for weak stability of the hairpin probe, leading to high background signals. When the length was extended to 15 nt, the strong duplex affinity hindered the primer probe from invading stacking, resulting in the inhibited CRSPR−Cas activity. Therefore, we chose a 12 nt hairpin probe for this study.

Tunable Sensitivity by Regulating the Loop Length of LP. Inspired by the intrinsically disordered domains in proteins, we propose to rationally design intrinsically disordered domains in the Y-shaped DNA scaffold to finely regulate its capture property through an entropic contribution. As shown in Figure 2A, we have designed a set of LP variants (LP0, LP5, LP15), in which we altered the loop length of the LP (dashed region) that connects the two recognition regions. To prevent nonspecific triplex-forming interactions between the duplex structures and the linker, a 5-nt sequence (5′-CTTTG-3′) was repeated to reduce the abundance of cytosines in the loop.[45]

To obtain a deeper comprehension of how the length of the loop impacts the LP binding affinity in capturing DNA tile onto the electrode surface, we examined thermal melting curves (Figure 2B) to measure the entropic contribution of various loop segments. We note that due to the loop-related modulation of the DNA substrate affinity, as the length of the loop increases, there is a decrease in melting temperatures as the entropy from the loop destabilizes the Y-shaped DNA (Figure S9). Interestingly, LP variants would have the same enthalpic contribution in their binding event since they differ only in the length of the loop region while sharing the same recognition region (Figures 2C and S10 and Table S2). This was evidenced by the identical slope in the van't Hoff plots in all tested variants. Importantly, the obtained intercept significantly increased with the increase of loop length (Figures 2C and S11 and Table S3), indicating that loop insertion manipulates the entropy of the system. Therefore, it can be inferred that the thermodynamic stability of the Y-shaped DNA scaffold can be regulated by distinct entropic contributions coming from the diverse loop region.

To examine the impact of the entropic contribution associated with the loop region on the sensitivity of the proposed method, we tested all variants in the presence of miR-31. As demonstrated in Figure 3A−C, the current intensity gradually reduced as the miR-31 concentration increased, between 0.1 fM and 100 nM, for all variants. LP0 (Figure 3D), LP5 (Figure 3E), and LP15 (Figure 3F) each reached a plateau at 0.1, 1, and 100 nM, respectively. It is noteworthy that LP0 exhibited a low LOD down to 0.31 fM (Figure 3G) based on the rule of S/N = 3, which is much lower than those of LP5 (32 fM, Figure 3H) and LP15 (0.56 pM, Figure 3I), suggesting that the enhanced entropic contribution reduced the sensitivity. As compared to previously reported methods, this proposed DNA tile and invading stacking primer-assisted CRISPR−Cas12a amplification strategy exhibited better performance with low sensitivity for miRNA detection (Table S4). We normalized the current responses for miR-31 detection and fit the curves by using the Hill equation. Consequently, we can obtain the K_d value from the fitting equation and determine the dynamic range, which is defined as the miR-31 concentrations where the normalized intensity is between 10 and 90%. Therefore, the dynamic range can be obtained by DNA tile and invading stacking primer-assisted CRISPR−Cas12a amplification with an ∼ 3000-fold, ∼ 2200-fold, and ∼3200-fold range of target concentrations (Figure 4A), which are much wider than the theoretical 81-fold range by the single-site binding mechanism without amplification. The entropic contribution tuned by the loop of LP induced a significant enhancement in binding affinity and regulated the K_d value from 0.73 pM to 0.07 nM (Figure 4B). Beyond the success of achieving a tunable dynamic range, we attempted to extend the dynamic range by the addition of a

https://doi.org/10.1021/acs.analchem.3c02603
Anal. Chem. XXXX, XXX, XXX−XXX

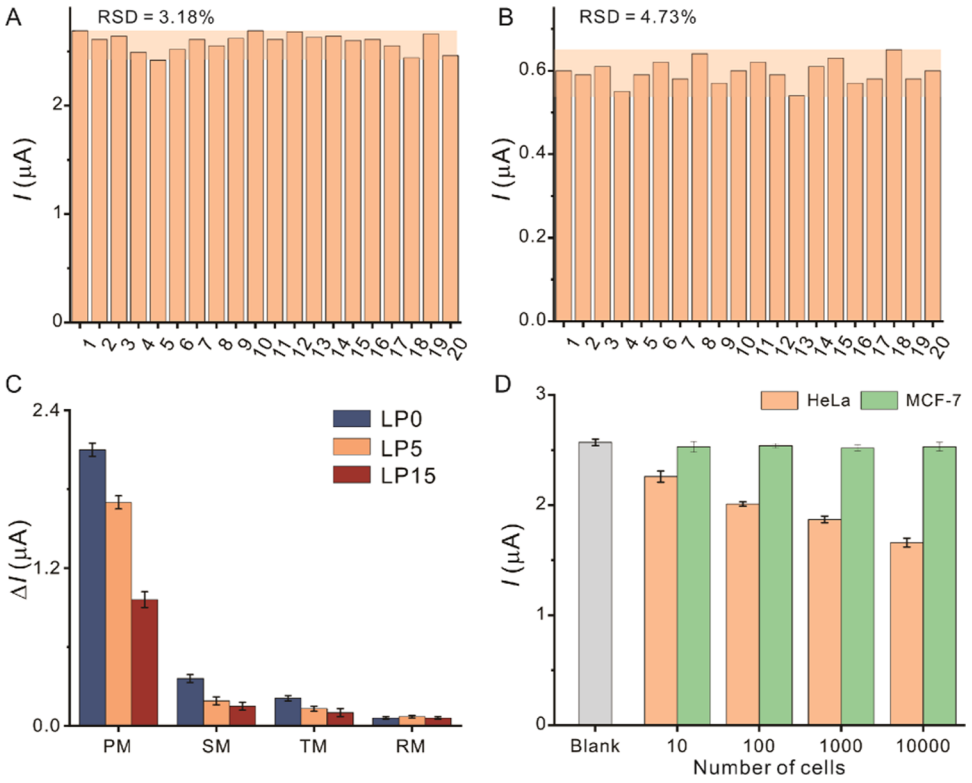


Figure 5. Reproducibility of the proposed biosensor (A) without and (B) with 100 pM miR-31 by 20 individual measurements. (C) Selectivity test of the proposed biosensor. The final concentrations for PM, SM, TM, and RM are 0.1 5, 5, and 5 nM, respectively. (D) Practical applicability of the proposed biosensor for detecting different concentrations of cancer cells. Error bars indicate the standard deviation of three replicates.

mixture of LP0 and LP15 at a ratio of 1:3. As shown in Figure S12, the intensity was observed to decline with the addition of target. The mixed linker probe exhibited a wide linear range of ~270,000-fold (Figures 4C and S13). The obtained LOD is down to 0.52 fM with R^2 = 0.9866 (Figure S14). Taken together, we can finely modulate the sensitivity and dynamic range in a controlled fashion using LP with different loop domains.

Investigation of Reproducibility and Selectivity. The performance of the biosensing platform was further assessed by examining the selectivity and reproducibility of the electrochemical biosensor. Initially, the reproducibility of the biosensor was evaluated by 20 individual measurements that were prepared without (Figure 5A) and with (Figure 5B) miR-31 (100 pM) under identical experimental conditions. The obtained relative standard deviations (RSDs) were 3.18 and 4.73%, indicating excellent reproducibility of the sensor. Additionally, control groups without (Figure S15A) and with (Figure S15B) the same miR-31 concentration (100 pM) were evaluated after 5 days at 4 °C, and the RSDs were found to be 4.29 and 4.97%, respectively, further confirming that the fabricated biosensor has desirable reproducibility.

To assess the selectivity of the method, various types of miRNAs were analyzed under the same conditions including a single-based mismatch miRNA (SM), a three-based mismatch miRNA (TM), and a random miRNA (RM). By comparing the alteration in current intensities of different target miRNAs at varying concentrations, it was observed that the detected ΔI from perfectly matched (PM) targets was stronger than that from SM, TM, and RM (Figure 5C). These findings demonstrate that the system exhibits remarkable specificity in distinguishing miRNAs with a single-based mismatch.

Practical Applicability of the Proposed Biosensor. To evaluate the feasibility of the proposed electrochemical biosensor in practical samples, recovery experiments were carried out. Varying concentrations of 0.50, 5.00, and 50.00 pM miR-31 were added to the diluted serum (100-fold) samples. By profiling the electrochemical intensities of all samples, the recoveries were obtained ranging from 95.4 to 107.1% with an RSD of less than 5% (Table S5), indicating that the proposed biosensing method is promising in real sample testing.

To assess the practicality of the electrochemical biosensor in evaluating miR-31 in a complex biological matrix, we examined the electrochemical response to miR-31 from MCF-7 and HeLa cells were examined. Figure 5D indicates that the electrochemical signal response considerably decreased as the number of Hela cells grew, indicating the high expression of miR-31 in these cells. Conversely, the current response in MCF-7 cells was insignificantly changed, indicating low miR-31 expression. These findings aligned with previous reports in the literature,[46] suggesting that the electrochemical biosensor has significant potential to monitor the miR-31 expression in cancer cells. The expression level of miR-31 was determined in MCF-7 and HeLa cells by using qRT-PCR. Figure S16 shows that miR-31 is overexpressed in HeLa cells compared with that in MCF-7 cells, consistent with the findings in Figure 5D. Additionally, there were no significant differences in the quantitation of the relative miR-31 expression levels between the two methods, indicating the high accuracy of the proposed system.

https://doi.org/10.1021/acs.analchem.3c02603
Anal. Chem. XXXX, XXX, XXX−XXX

CONCLUSIONS

In summary, we have demonstrated that the proposed DNA tile and invading stacking primer-assisted CRISPR−Cas12a amplification-based electrochemical biosensor presents a novel and sensitive approach to detecting miR-31 with tunable dynamic ranges. By incorporating an entropy-controlled Y-shaped DNA scaffold, we were able to tune the dynamic range of the target detection by adjusting the length of the loop region of the LP that connects the DNA tetrahedron and DNA tile. Our findings reveal that shorter loops result in lower entropy and LOD, indicating a higher sensitivity for miRNA detection, while longer loops increase the entropic contribution and lower sensitivity. Despite the alteration of the system entropy, the enthalpy remains the same since the loop region is not involved in the recognition reactions. Consequently, our proposed biosensor offers several advantages, including the following: (i) multiple amplification strategy combining ISPSA, CRISPR−Cas12a, and DNA tile improves the sensitivity and efficiency; (ii) tunable LOD from 0.31 fM to 0.56 pM; and (iii) tunable detection range from ∼2200-fold to ∼270,000-fold. Future experiments will investigate the potential for electrochemical biosensors with stimuli-responsive probes capable of arbitrarily expanding or narrowing dynamic ranges by the programmable regulation of unique DNA structures. The proposed method can be used as a universal approach by simply replacing the target-responsive hairpin probe for detecting various targets, including nucleic acids, ions, proteins, small molecules, and cells. Further research will focus on the development of signal-on biosensors, which might be more favorable for practical applications. Benefiting from the programmable capability of the nucleic acid, the proposed strategy can easily be adapted to determine other biomarkers for clinical diagnosis by substituting the specific recognition regions with appropriate responsive sequences or aptamer sequences.

ASSOCIATED CONTENT

Supporting Information

The Supporting Information is available free of charge at https://pubs.acs.org/doi/10.1021/acs.analchem.3c02603.

Experimental section; PAGE analysis; AFM image of DNA tile; ACV responses of control experiment; optimizing experiments; melting temperature, enthalpic and entropic contribution of different LP variants; ACV response and plots of the proposed biosensor using a mixture of LP0 and LP15; oligonucleotide sequences; and calculated enthalpic and entropic contribution using different LP variants (PDF)

AUTHOR INFORMATION

Corresponding Author

Zhong Feng Gao − *Key Laboratory of Interfacial Reaction & Sensing Analysis in Universities of Shandong, School of Chemistry and Chemical Engineering, University of Jinan, Jinan 250022, P. R. China;* orcid.org/0000-0002-4667-6212; Email: chm_gaozf@ujn.edu.cn

Authors

Huan Wang − *Key Laboratory of Interfacial Reaction & Sensing Analysis in Universities of Shandong, School of Chemistry and Chemical Engineering, University of Jinan, Jinan 250022, P. R. China;* orcid.org/0000-0002-0855-1427

Yan Lei Li − *Key Laboratory of Interfacial Reaction & Sensing Analysis in Universities of Shandong, School of Chemistry and Chemical Engineering, University of Jinan, Jinan 250022, P. R. China*

Ya Jie Fan − *Key Laboratory of Analytical Science and Technology of Hebei Province, College of Chemistry and Materials Science, Hebei University, Baoding 071002, P. R. China*

Jiang Xue Dong − *Key Laboratory of Analytical Science and Technology of Hebei Province, College of Chemistry and Materials Science, Hebei University, Baoding 071002, P. R. China*

Xiang Ren − *Key Laboratory of Interfacial Reaction & Sensing Analysis in Universities of Shandong, School of Chemistry and Chemical Engineering, University of Jinan, Jinan 250022, P. R. China;* orcid.org/0000-0002-4321-4282

Hongmin Ma − *Key Laboratory of Interfacial Reaction & Sensing Analysis in Universities of Shandong, School of Chemistry and Chemical Engineering, University of Jinan, Jinan 250022, P. R. China;* orcid.org/0000-0002-7061-8944

Dan Wu − *Key Laboratory of Interfacial Reaction & Sensing Analysis in Universities of Shandong, School of Chemistry and Chemical Engineering, University of Jinan, Jinan 250022, P. R. China;* orcid.org/0000-0002-8732-5988

Qin Wei − *Key Laboratory of Interfacial Reaction & Sensing Analysis in Universities of Shandong, School of Chemistry and Chemical Engineering, University of Jinan, Jinan 250022, P. R. China;* orcid.org/0000-0002-3034-8046

Fan Xia − *Engineering Research Center of Nano-Geomaterials of Ministry of Education, Faculty of Materials Science and Chemistry, China University of Geosciences, Wuhan 430074, P. R. China;* orcid.org/0000-0001-7705-4638

Complete contact information is available at: https://pubs.acs.org/10.1021/acs.analchem.3c02603

Notes

The authors declare no competing financial interest.

ACKNOWLEDGMENTS

This work was supported by the National Natural Science Foundation of China (22176080, 22204060, and 22274062), the Natural Science Foundation of Shandong Province (ZR2023YQ015), the Natural Science Foundation of Hebei Province (B2019201397), and the Project funded by China Postdoctoral Science Foundation (2020M670678).

REFERENCES

(1) Ruvkun, G. *Science* **2006**, *311*, 36−37.
(2) Ji, D.; Guo, M.; Wu, Y.; Liu, W.; Luo, S.; Wang, X.; Kang, H.; Chen, Y.; Dai, C.; Kong, D.; Ma, H.; Liu, Y.; Wei, D. *J. Am. Chem. Soc.* **2022**, *144*, 13526−13537.
(3) Liu, X.; Xiang, J.; Cheng, H.; Wang, Y.; Li, F. *Chin. J. Chem.* **2022**, *40*, 2808−2814.
(4) Van den Berg, M. M. J.; Krauskopf, J.; Ramaekers, J. G.; Kleinjans, J. C. S.; Prickaerts, J.; Bried, J. J. *Prog. Neurobiol.* **2020**, *185*, No. 101732.
(5) Jeon, J.; Olkhov-Mitsel, E.; Xie, H.; Yao, C. Q.; Zhao, F.; Jahangiri, S.; Cuizon, C.; Scarcello, S.; Jeyapala, R.; Watson, J. D.; Fraser, M.; Ray, J.; Commisso, K.; Loblaw, A.; Fleshner, N. E.;

Bristow, R. G.; Downes, M.; Vesprini, D.; Liu, S.; Bapat, B. J.; Boutros, P. C. *JNCI, J. Natl. Cancer Inst.* **2020**, *112*, 247−255.
(6) Lee, T. J.; Yuan, X.; Kerr, K.; Yoo, J. Y.; Kim, D. H.; Kaur, B.; Eltzschig, H. K. *Pharmacol. Rev.* **2020**, *72*, 639−667.
(7) Drees, E. E. E.; Pegtel, D. M. *Trends Cancer* **2020**, *6*, 910−923.
(8) Causa, F.; Aliberti, A.; Cusano, A. M.; Battista, E.; Netti, P. A. *J. Am. Chem. Soc.* **2015**, *137*, 1758−1761.
(9) Joshi, G. K.; Deitz-McElyea, S.; Liyanage, T.; Lawrence, K.; Mali, S.; Sardar, R.; Korc, M. *ACS Nano* **2015**, *9*, 11075−11089.
(10) Chen, D.; Huang, W.; Zhang, Y.; Chen, B.; Tan, J.; Yang, Y.; Yuan, Q. *Angew. Chem., Int. Ed.* **2023**, *62*, No. e2023042.
(11) Gong, S.; Zhang, S.; Lu, F.; Pan, W.; Li, N.; Tang, B. *Anal. Chem.* **2021**, *93*, 11899−11909.
(12) Qing, M.; Chen, S. L.; Sun, Z.; Fan, Y.; Luo, H. Q.; Li, N. B. *Anal. Chem.* **2021**, *93*, 7499−7507.
(13) Zhao, Q.; Pan, B.; Long, W.; Pan, Y.; Zhou, D.; Luan, X.; He, B.; Wang, Y.; Song, Y. *Nano Lett.* **2022**, *22*, 9714−9722.
(14) Liu, J.; Chen, J.; Wu, D.; Huang, M.; Chen, J.; Pan, R.; Wu, Y.; Li, G. *Anal. Chem.* **2021**, *93*, 10167−10174.
(15) Qin, N.; Deng, L.; Wang, M.; Hun, X. *ACS Appl. Nano Mater.* **2021**, *4*, 10701−10707.
(16) Gao, Z. F.; Zheng, L. L.; Dong, L. M.; Li, J. Z.; Shen, Y.; Chen, P.; Xia, F. *Anal. Chem.* **2022**, *94*, 6371−6379.
(17) Zhang, K.; Fan, Z.; Ding, Y.; Xie, M. *Chem. Eng. J.* **2022**, *429*, No. 132472.
(18) Wu, L.; Wang, X.; Wu, X.; Xu, S.; Liu, M.; Cao, X.; Tang, T.; Huang, X.; Huang, H. *ACS Appl. Mater. Interfaces* **2022**, *14*, 50534−50542.
(19) Lin, X.; Li, C.; Meng, X.; Yu, W.; Duan, N.; Wang, Z.; Wu, S. *J. Hazard. Mater.* **2022**, *433*, No. 128750.
(20) Lin, C.; Liu, Y.; Rinker, S.; Yan, H. *ChemPhysChem* **2006**, *7*, 1641−1647.
(21) Evans, C. G.; Winfree, E. *Chem. Soc. Rev.* **2017**, *46*, 3808−3829.
(22) Zhang, D. Y.; Hariadi, R. F.; Choi, H. M.; Winfree, E. *Nat. Commun.* **2013**, *4*, No. 1965.
(23) Wei, B.; Dai, M.; Yin, P. *Nature* **2012**, *485*, 623−626.
(24) Li, J.; Fan, C.; Pei, H.; Shi, J.; Huang, Q. *Adv. Mater.* **2013**, *25*, 4386−4396.
(25) Chao, J.; Liu, H.; Su, S.; Wang, L.; Huang, W.; Fan, C. *Small* **2014**, *10*, 4626−4635.
(26) Li, S.; Li, C.; Wang, Y.; Li, H.; Xia, F. *Anal. Chem.* **2020**, *92*, 13427−13433.
(27) Setia, U.; Gross, P. A. *J. Infect. Dis.* **1976**, *134*, S125−S129.
(28) Ricci, F.; Vallée-Bélisle, A.; Simon, A. J.; Porchetta, A.; Plaxco, K. W. *Acc. Chem. Res.* **2016**, *49*, 1884−1892.
(29) Zou, L.; Wu, Z.; Liu, X.; Zheng, Y.; Mei, W.; Wang, Q.; Yang, X.; Wang, K. *Anal. Chem.* **2020**, *92*, 11953−11959.
(30) Pan, J.; Xu, W.; Li, W.; Chen, S.; Dai, Y.; Yu, S.; Zhou, Q.; Xia, F. *Anal. Chem.* **2023**, *95*, 420−432.
(31) Carpenter, C. C. J.; Fischl, M. A.; Hammer, S. M.; Hirsch, M. S.; Jacobsen, D. M.; Katzenstein, D. A.; Montaner, J. S. G.; Richman, D. D.; Saag, M. S.; Schooley, R. T.; Thompson, M. A.; Vella, S.; Yeni, P. G.; Volberding, P. A. *JAMA* **1997**, *277*, 1962−1969.
(32) Huang, C. Y.; Ferrell, J. E., Jr. *Proc. Natl. Acad. Sci. U.S.A.* **1996**, *93*, 10078−10083.
(33) Tsai, C. J.; del Sol, A.; Nussinov, R. *Mol. BioSyst.* **2009**, *5*, 207−216.
(34) Cui, Q.; Karplus, M. *Protein Sci.* **2008**, *17*, 1295−1307.
(35) Bloom, J. D.; Arnold, F. H. *Proc. Natl. Acad. Sci. U.S.A.* **2009**, *106*, 9995−10000.
(36) Porchetta, A.; Vallée-Bélisle, A.; Plaxco, K. W.; Ricci, F. *J. Am. Chem. Soc.* **2012**, *134*, 20601−20604.
(37) Mei, W.; Zhou, Y.; Xia, L.; Liu, X.; Huang, W.; Wang, H.; Zou, L.; Wang, Q.; Yang, X.; Wang, K. *ACS Sens.* **2023**, *8*, 381−387.
(38) Zheng, L. L.; Li, J. Z.; Wen, M.; Xi, D.; Zhu, Y.; Wei, Q.; Zhang, X. B.; Ke, G.; Xia, F.; Gao, Z. F. *Sci. Adv.* **2023**, *9*, No. eadf5868.
(39) Lu, N.; Pei, H.; Ge, Z. L.; Simmons, C. R.; Yan, H.; Fan, C. H. *J. Am. Chem. Soc.* **2012**, *134*, 13148−13151.
(40) Edblom, E. C.; Orban, M.; Epstein, I. R. *J. Am. Chem. Soc.* **1986**, *108*, 2826−2830.
(41) Li, X.; Wang, G.; Zhang, Q.; Liu, Y.; Sun, T.; Liu, S. *J. Colloid Interface Sci.* **2022**, *615*, 732−739.
(42) Mergny, J. L.; Lacroix, L. *Oligonucleotides* **2003**, *13*, 515−537.
(43) Ge, Z.; Lin, M.; Wang, P.; Pei, H.; Yan, J.; Shi, J.; Huang, Q.; He, D.; Fan, C.; Zuo, X. *Anal. Chem.* **2014**, *86*, 2124−2130.
(44) Lin, M.; Wen, Y.; Li, L.; Pei, H.; Liu, G.; Song, H.; Zuo, X.; Fan, C.; Huang, Q. *Anal. Chem.* **2014**, *86* (5), 2285−2288.
(45) Wang, S.; Booher, M. A.; Kool, E. T. *Biochemistry* **1994**, *33*, 4639−4644.
(46) Sayers, J.; Payne, R. J.; Winssinger, N. *Chem. Sci.* **2018**, *9*, 896−903.

https://doi.org/10.1021/acs.analchem.3c02603
Anal. Chem. XXXX, XXX, XXX−XXX